Ice crust - convective ocean model

Jakub Kvorka[1] and Ondřej Čadek[1]

[1]Charles University, Faculty of Mathematics and Physics, Department of Geophysics

29.3.2023

Overview: Topography and shape of Titan

Figure: The shape (first row) and the topography (second row) of Titan up to degree 5 and its zonal part including the degree/order 2/2 [Corlies et al., 2017, Durante et al., 2019].

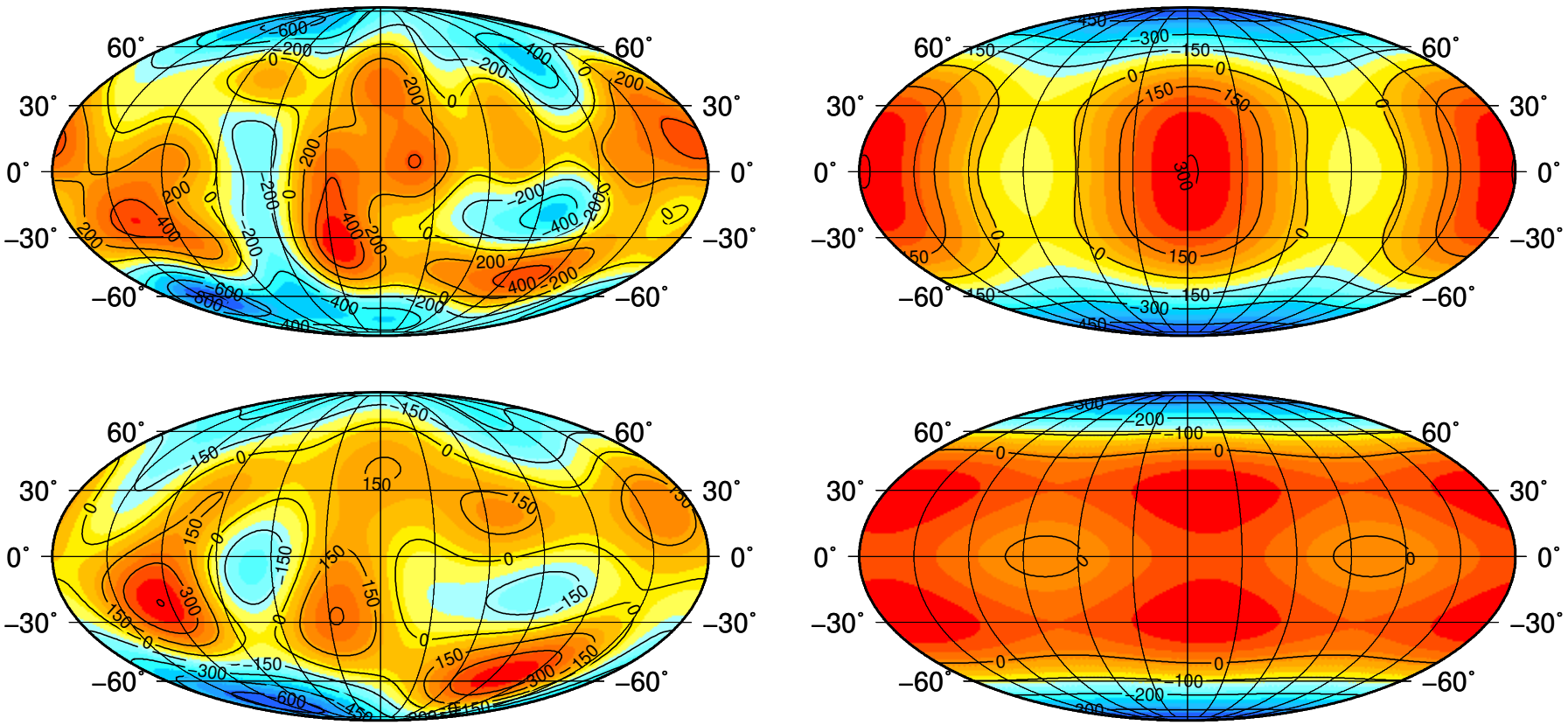

Overview: Topography inversion, Kvorka et al. [2018]

Figure: Left: Simple model for a topography variation driven by the variations of the heat flux at the ice-ocean interface. Right: Inverse problem solution [Kvorka et al., 2018].

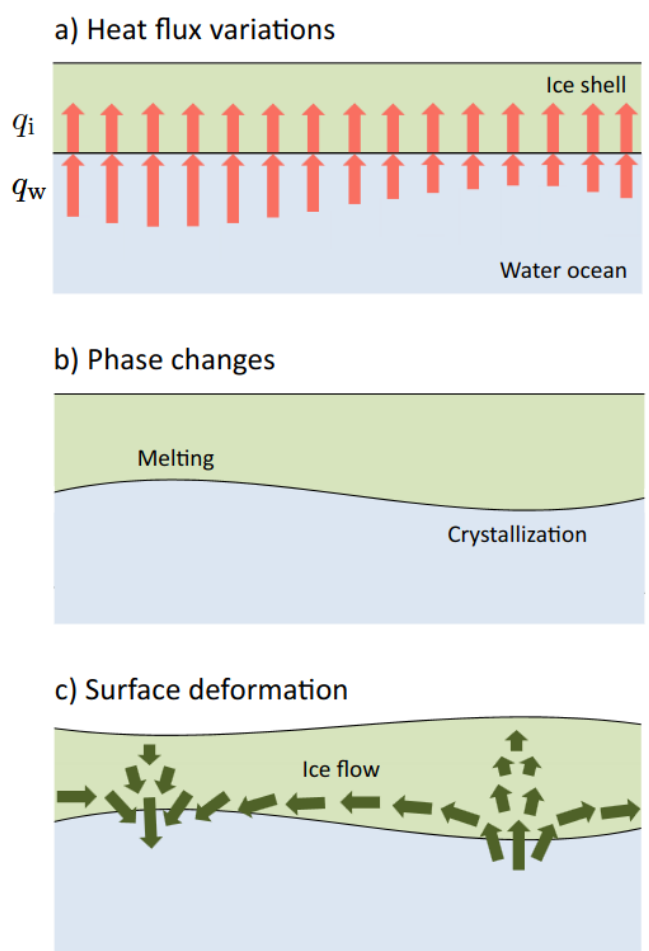

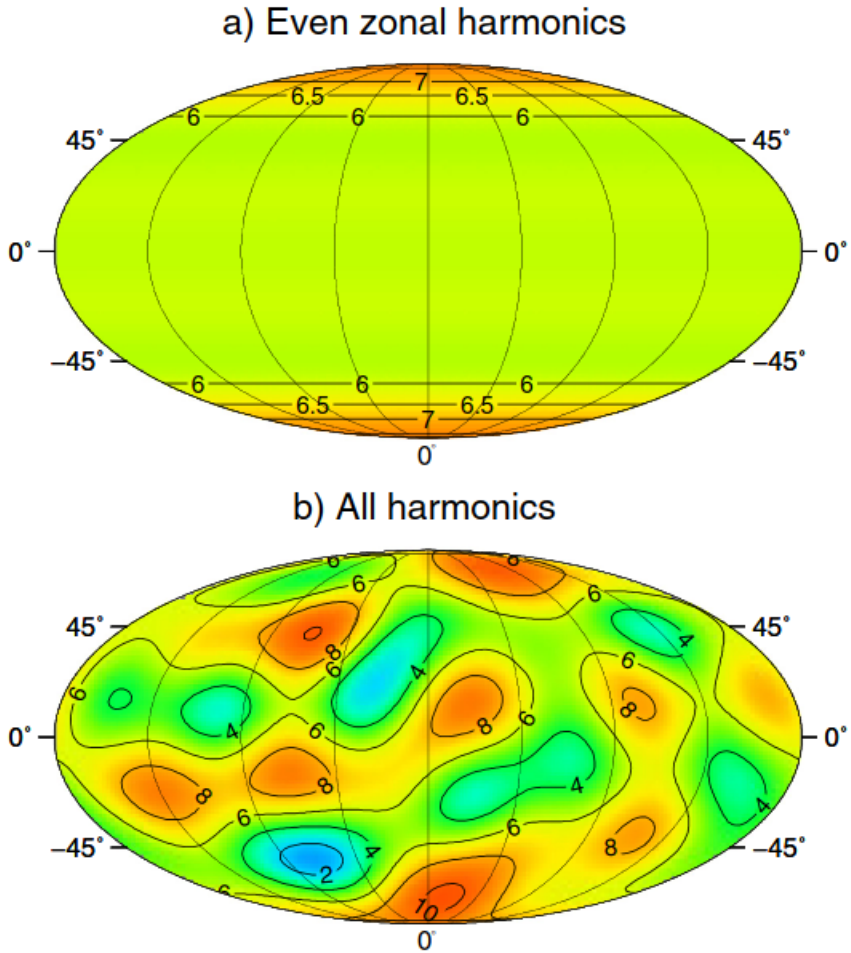

Overview: Rotating convection

Figure: Temperature fluctuations profile in rotating convection models. The influence of the Coriolis force is rising from the picture (a, non-rotating case) to the picture (d, rapidly rotating case) [Gastine et al., 2016].

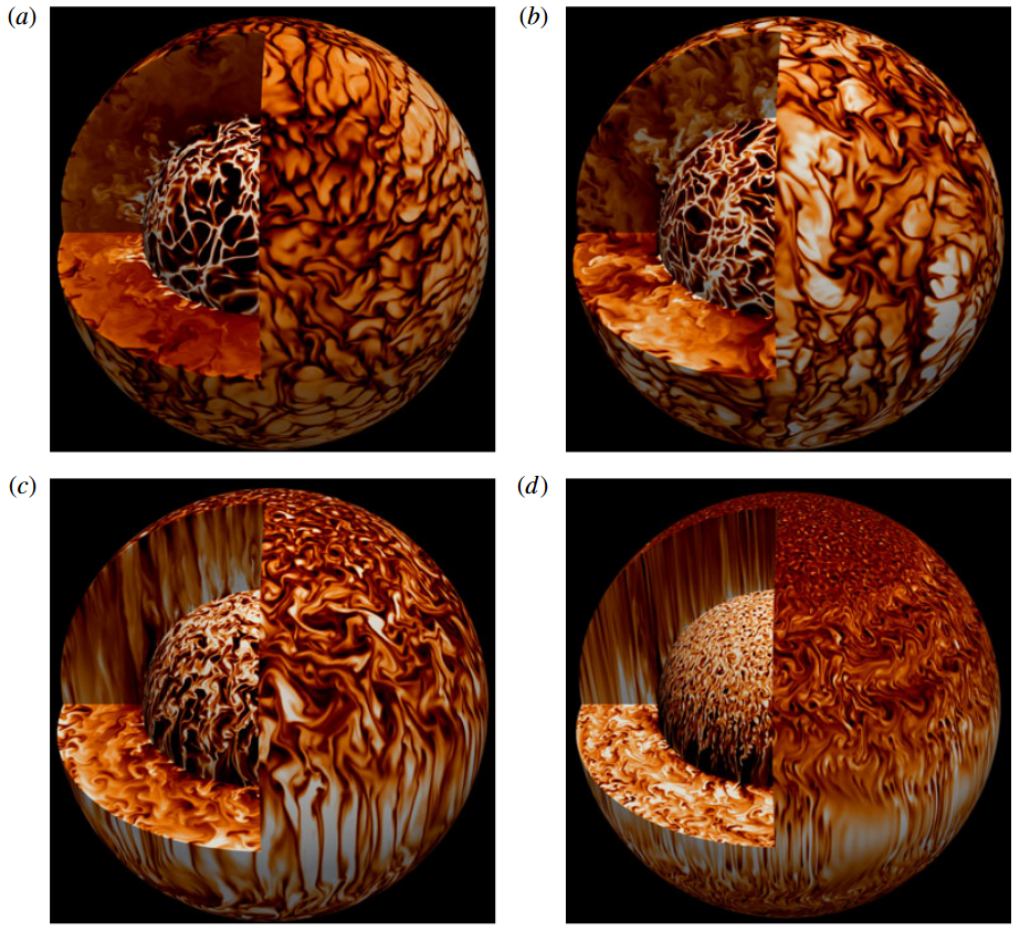

Overview: Rotating convection

Figure: Heat flux variation, [Amit et al., 2020].

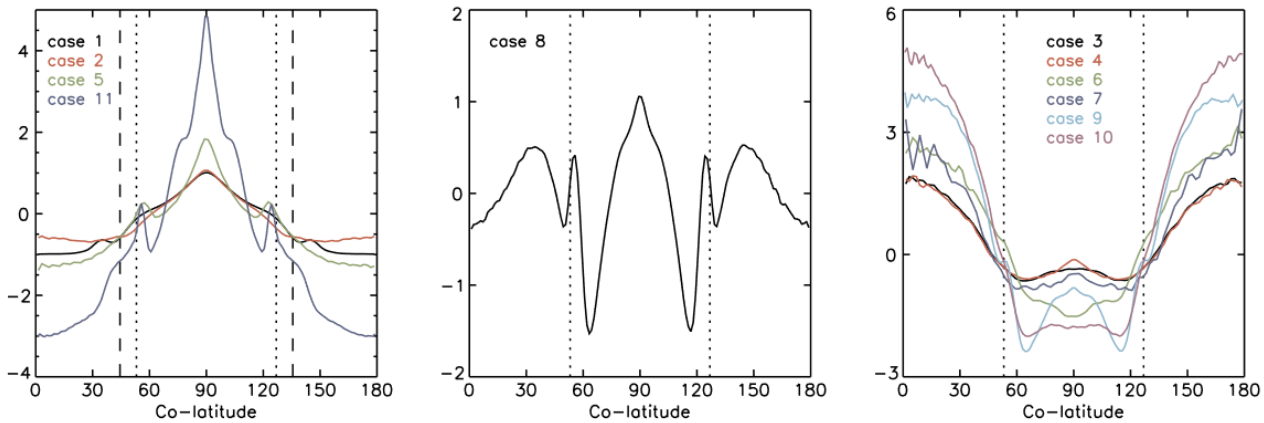

Figure: Topography vs heat flux, [Kvorka and Čadek, 2022].

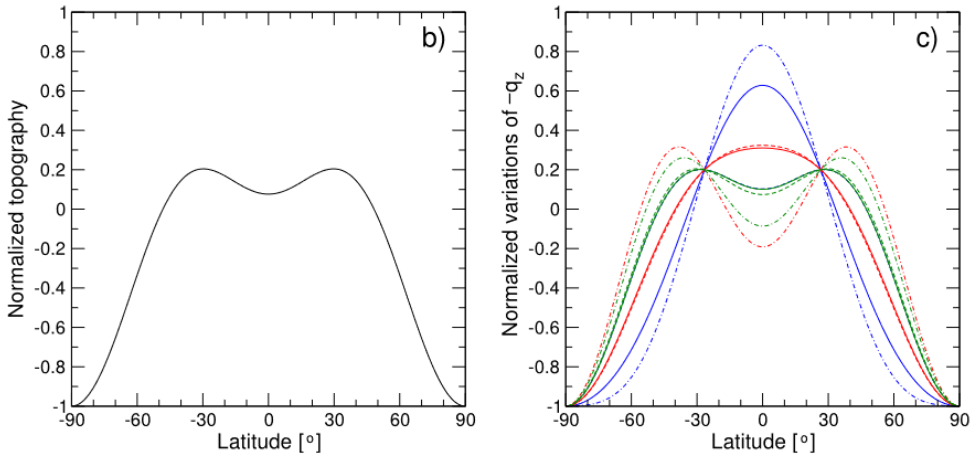

Overview: Heat advection along boundary

Figure: Boundary deformation and heat advection, [Labrosse et al., 2018].

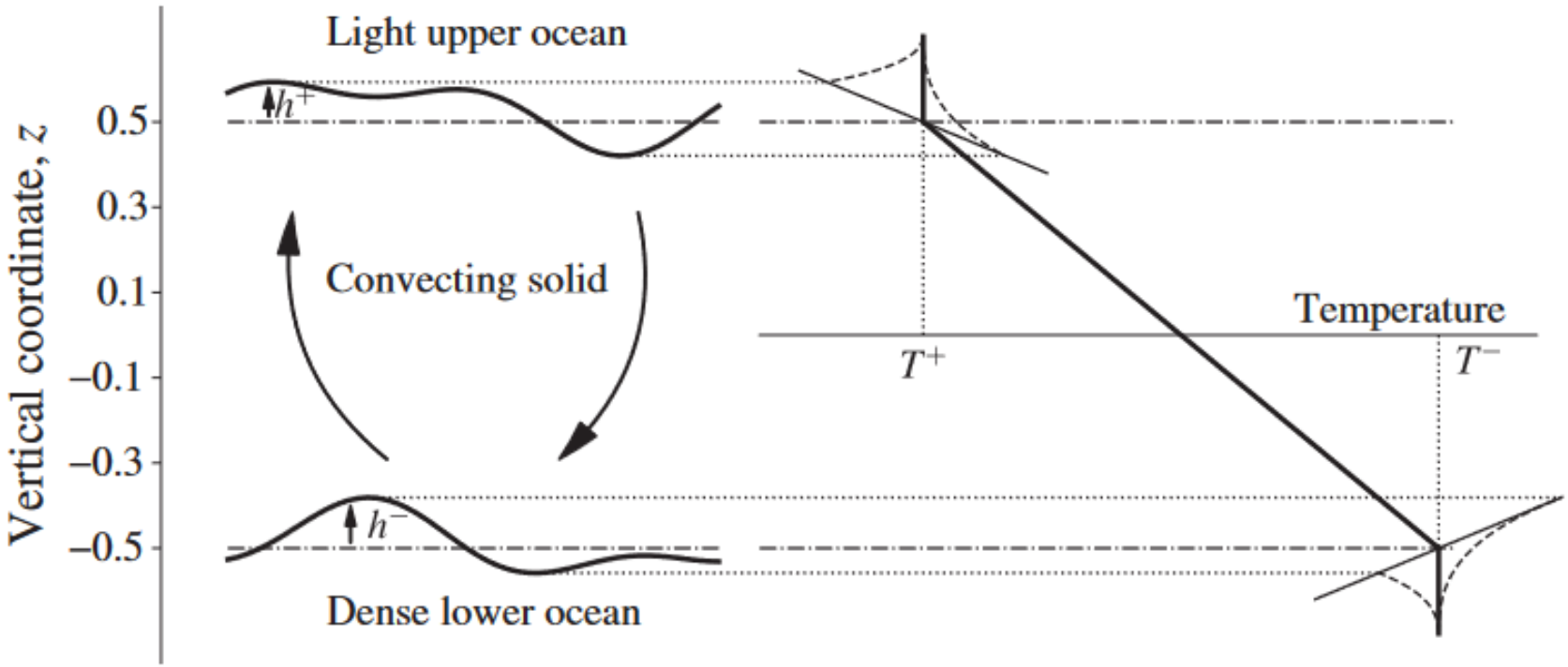

- proposal for the heat flux: $q \approx q_o - \gamma(v_o, C_L)u$

Overview: Heat advection along boundary

Figure: Boundary deformation and heat advection, [Kihoulou et al., 2023].

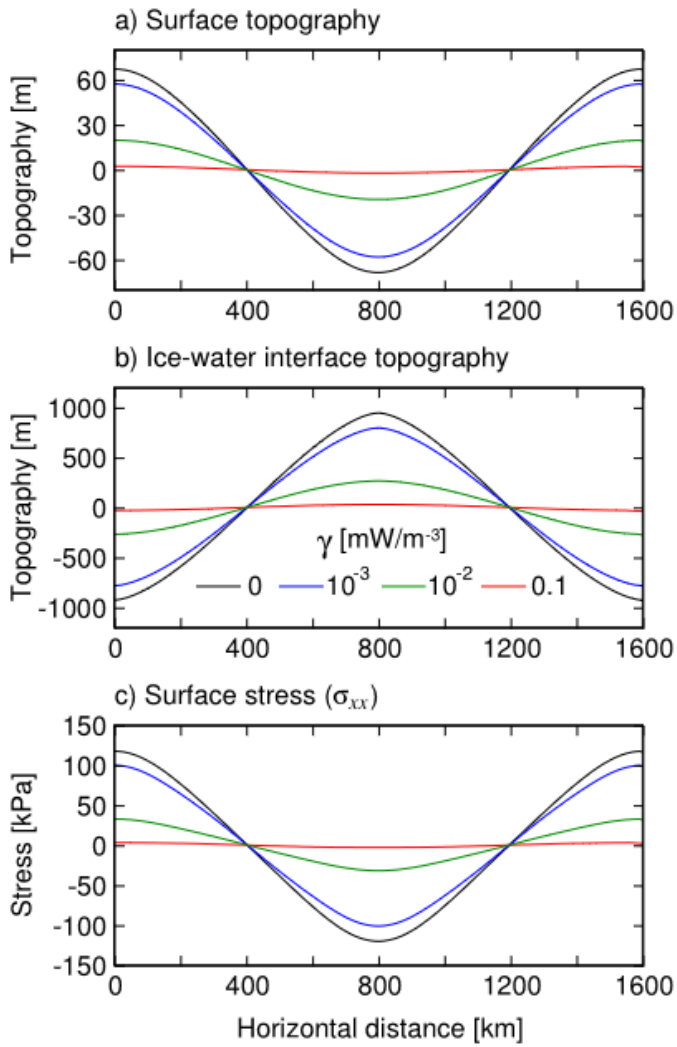

Foundations: Ice shell

- the model describing the viscous deformation of an ice shell [Kvorka et al., 2018, Čadek et al., 2019] with possible influence of heat advection along a phase interface [Kihoulou et al., 2023]

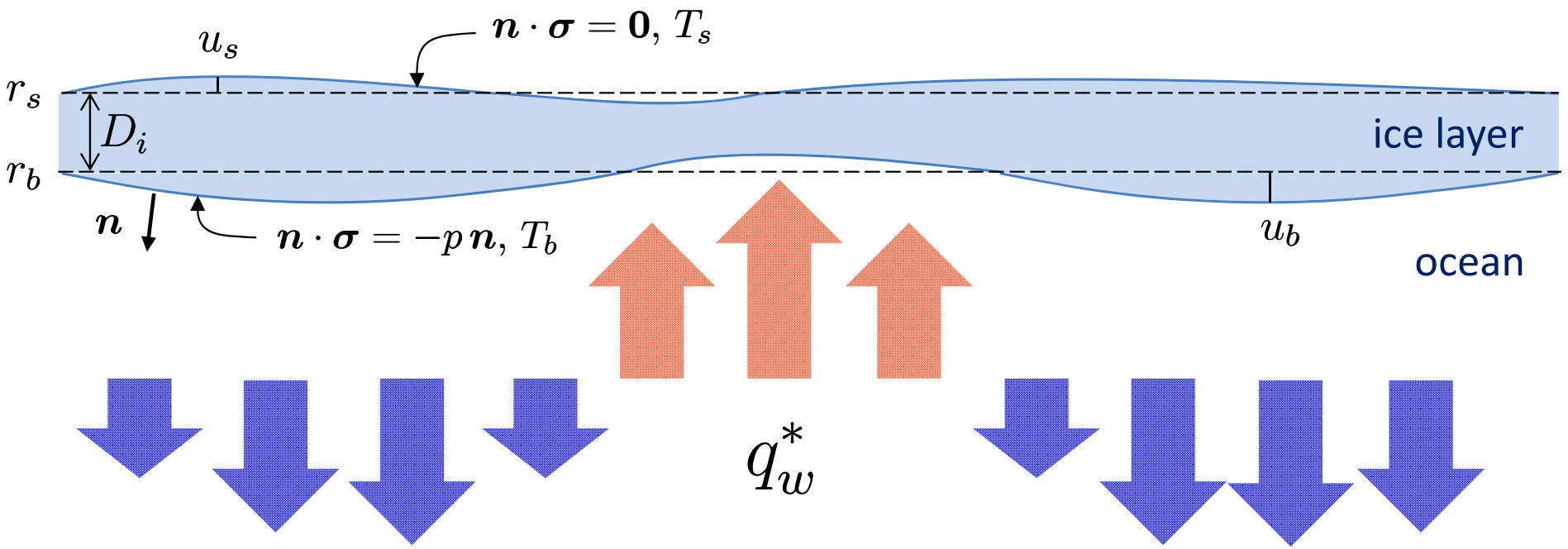

Foundations: Ice shell, governing equations

$$\nabla \cdot \boldsymbol{v}_i = 0 \tag{1}$$

$$\nabla \cdot \boldsymbol{\sigma}_i + \rho_i g \alpha_i (T_i - T_{i0}) \boldsymbol{e}_r = \rho_i (g \boldsymbol{e}_r - \nabla V) \tag{2}$$

$$\boldsymbol{\sigma}_i = -p_i \boldsymbol{I} + \eta_i \left(\nabla \boldsymbol{v}_i + (\nabla \boldsymbol{v}_i)^T \right) \tag{3}$$

$$\rho_i c_{pi} \frac{\partial T_i}{\partial t} = \nabla \cdot (\lambda_i \nabla T_i) - \rho_i c_{pi} \boldsymbol{v}_i \cdot \nabla T_i \tag{4}$$

$\boldsymbol{v}_i$ - velocity of the ice flow, $\boldsymbol{\sigma}_i$ - the Cauchy stress tensor, ρ_i - density of ice, g - gravitational acceleration, α_i - thermal expansivity of ice, T_i - temperature, T_{i0} - reference temperature, V - the self-gravitational potential and the potential of external forces, p_i - pressure, η_i - viscosity, c_{pi} - thermal capacity at constant pressure, λ_i - thermal conductivity

Foundations: Ice shell, boundary conditions

- surface of the ice shell: isothermal material boundary [Čadek et al., 2017]

$$T_i(r_s + u_s) = T_s \quad \ldots \quad T_i(r_s) + u_s \frac{\partial \overline{T}_i}{\partial r}(r_s) = T_s \tag{5}$$

$$\boldsymbol{n}\cdot\boldsymbol{\sigma}_i(r_s + u_s) = \boldsymbol{0} \quad \ldots \quad \boldsymbol{e}_r\cdot\boldsymbol{\sigma}_i(r_s) + \rho_i g u_s \boldsymbol{e}_r = \boldsymbol{0} \tag{6}$$

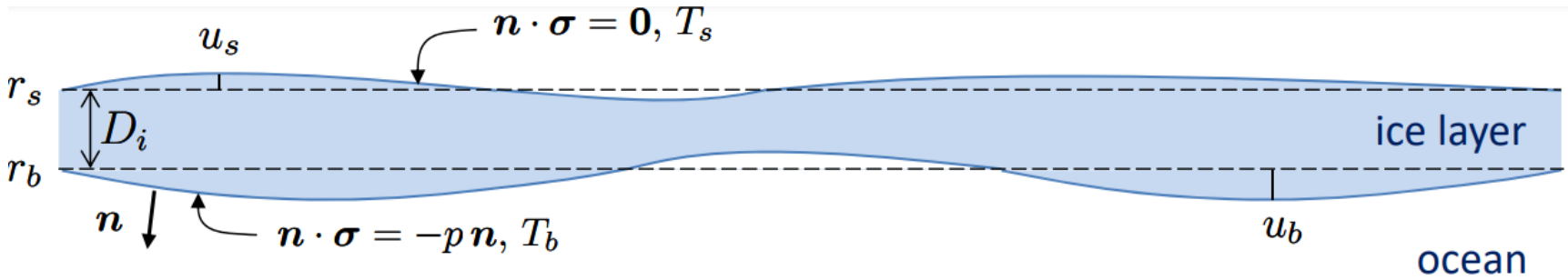

Foundations: Ice shell, boundary conditions

- ice/ocean interface: phase boundary [Kvorka et al., 2018]

$$T_i(r_b + u_b) = T_m(p(r_b + u_b)) \tag{7}$$

$$\boldsymbol{n}\cdot\boldsymbol{\sigma}(r_b + u_b) = -p_w(r_b + u_b)\boldsymbol{n} \tag{8}$$

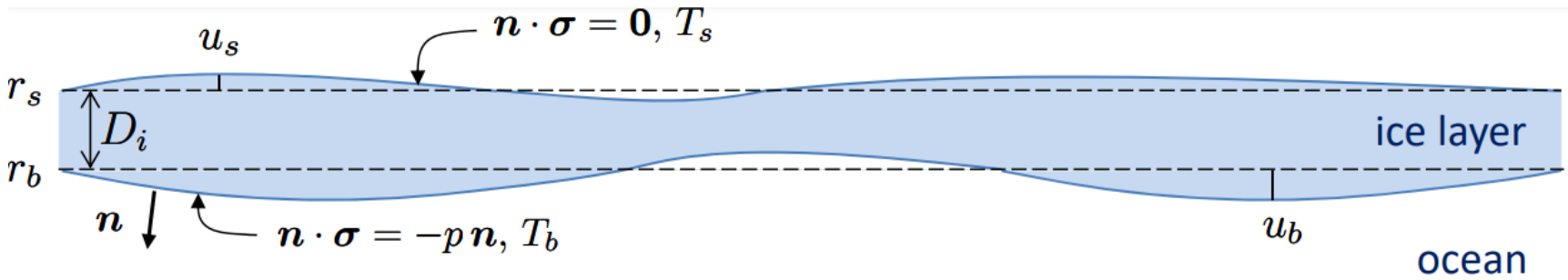

Foundations: Ice shell, boundary conditions

- ice/ocean interface: phase boundary [Kvorka et al., 2018, Čadek et al., 2019]

$$T_i(r_b) + u_b \frac{\partial \overline{T}_i}{\partial r}(r_b) = T_m(p_b) - \rho_w g t_b \frac{dT_m}{dp}(p_b) \tag{9}$$

$$-\boldsymbol{e}_r \cdot \boldsymbol{\sigma}_i(r_b) - (\rho_i - \rho_w) g u_b \boldsymbol{e}_r = p_b \boldsymbol{e}_r + \rho_w V(r_b) \boldsymbol{e}_r \tag{10}$$

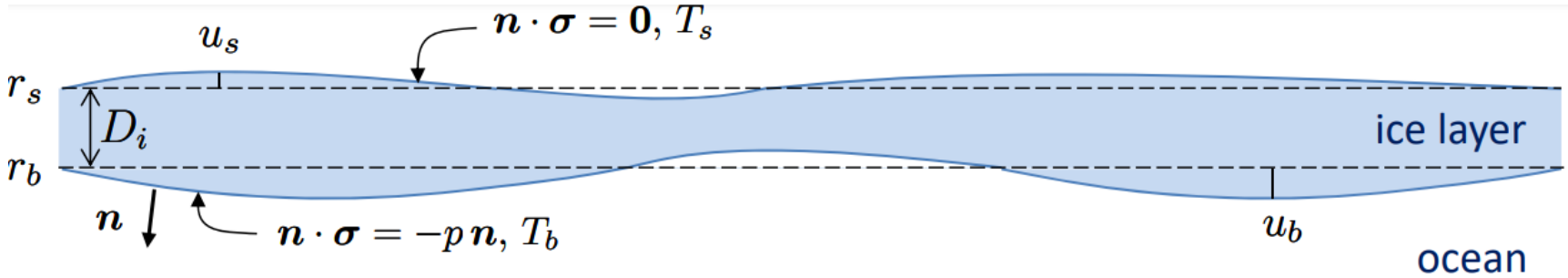

t_b - topography of the ice/ocean interface (distance from geoid [Čadek et al., 2021])

Boundary evolution

- the surface: evolution of material boundary [Dingemans, 1997]
- the ice/ocean interface: evolution involving the freezing/melting processes [Kvorka et al., 2018, Čadek et al., 2019] under the assumption on continuity of laterally averaged radial part of the heat flux $\overline{q}_{r,i} = \overline{q}_{r,w}$

$$\frac{\partial u_s(t)}{\partial t} = \boldsymbol{e}_r \cdot \boldsymbol{v}_i(t, r_s) \tag{11}$$

$$\frac{\partial u_b(t)}{\partial t} = \boldsymbol{e}_r \cdot \boldsymbol{v}_i(t, r_b) - \frac{\overline{q}_{r,i}(t, r_b)}{L\rho_i} \boldsymbol{e}_r \cdot [\boldsymbol{q}_i^*(t, r_b) - \boldsymbol{q}_w^*(t, r_b)] \tag{12}$$

Foundations: Water ocean, governing equations

- non-dimensional treatment [Schmitz and Tilgner, 2009, 2010]

$$\nabla \cdot \tilde{\boldsymbol{v}}_w = 0 \tag{13}$$

$$\frac{1}{Pr}\left(\frac{\partial \tilde{\boldsymbol{v}}_w}{\partial \tilde{t}} + \tilde{\boldsymbol{v}}_w \cdot \nabla \tilde{\boldsymbol{v}}_w\right) + \frac{2}{Ek}\boldsymbol{e}_z \times \tilde{\boldsymbol{v}}_w = -\nabla p_w + \nabla^2 \tilde{\boldsymbol{v}}_w + Ra\frac{\tilde{r}_b^2}{\tilde{r}^2}\tilde{T}_w \boldsymbol{e}_r \tag{14}$$

$$\frac{\partial \tilde{T}_w}{\partial \tilde{t}} + \tilde{\boldsymbol{v}}_w \cdot \nabla \tilde{T}_w = \nabla^2 \tilde{T}_w \tag{15}$$

$\tilde{\boldsymbol{v}}_w$ - ocean velocity, $\tilde{t}$ - dimensionless time, $\boldsymbol{e}_z$ - unit vector along the z axis, p_w - water pressure, $\tilde{r}$ - dimensionless radial coordinate, $\tilde{T}_w$ - ocean temperature

Foundations: Water ocean, control parameters

Considering $D_w = 500km$ and parameters relevant to Titan's ocean:

- Rayleigh number $Ra = \alpha_w g \Delta T D_w^3/(\kappa_w \nu_w) \approx$???
- $Ek = \nu_w/(\Omega D_w^2) \approx 2\times10^{-12}$, $Pr = \nu_w/\kappa_w \approx 10$

Rayleigh number estimate: $Q \approx 400GW$ from our model of the ice crust, $R_G^* = RaEk^{12/7}/Pr \approx 3.3$

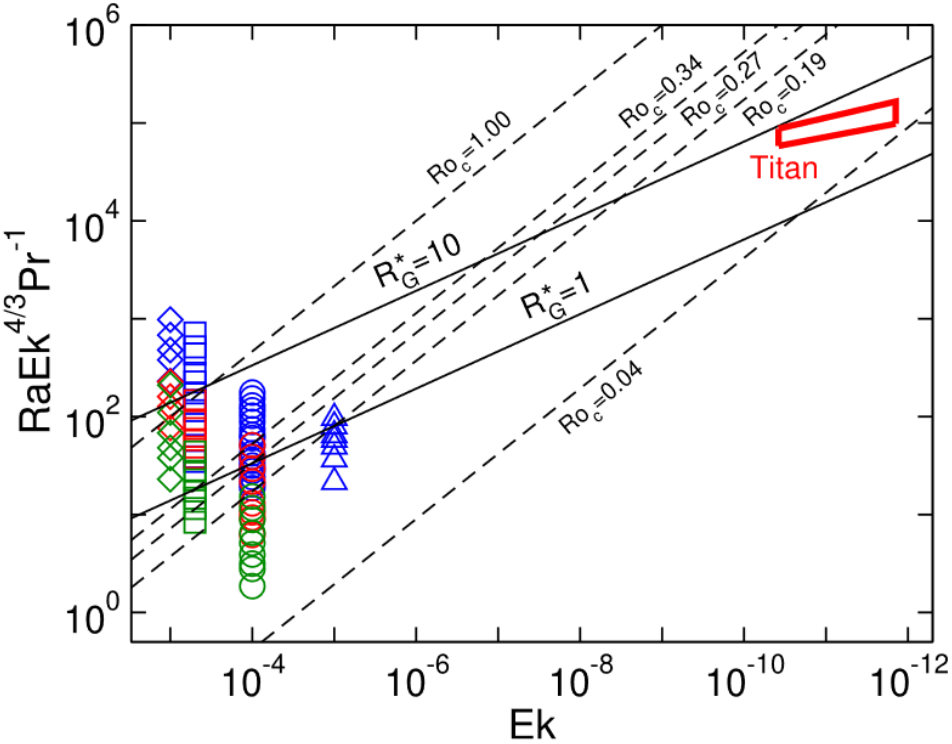

Foundations: Water ocean, boundary conditions I

- mass conservation at the boundary provides an estimate on ocean radial velocity [Slattery et al., 2007]

$$\rho_w \left(\boldsymbol{e}_r \cdot \boldsymbol{v}_w - \frac{\partial u_b}{\partial t} \right) = \rho_i \left(\boldsymbol{e}_r \cdot \boldsymbol{v}_i - \frac{\partial u_b}{\partial t} \right) \tag{16}$$

- $\boldsymbol{e}_r \cdot \boldsymbol{v}_i$: 1-1000 $mm/year$ [Kihoulou et al., 2023]
- $|\boldsymbol{v}_w|$: m/s [Soderlund, 2019, Kvorka and Čadek, 2022]
- mechanical boundary conditions: **impermeable stress-free boundary**

Foundations: Water ocean, boundary conditions II

- thermal boundary condition: **fixed temperature**

$$T_w(r_b + u_b) = T_m(p(r_b + u_b)) \tag{17}$$
$$T_w(r_c) = T_c \tag{18}$$

- by the same procedure as in the case of the ice shell we obtain

$$T_w(r_b) + u_b \frac{\partial \overline{T}_w}{\partial r}(r_b) = T_m(p_b) - \rho_w g t_b \frac{dT_m}{dp}(p_b) \tag{19}$$
$$T_w(r_c) = T_c \tag{20}$$

Foundations: Water ocean, boundary conditions III

- non-dimensional form of thermal boundary condition

$$\tilde{T}_w(\tilde{r}_b) = \frac{\tilde{r}_c}{\tilde{r}_b} Nu\tilde{u}_b - \frac{\rho_w g D_w}{\Delta \overline{T}} \frac{dT_m}{dp}(p_b)\tilde{t}_b \tag{21}$$

$$\tilde{T}_w(\tilde{r}_c) = 1 \tag{22}$$

- new non-dimensional parameter C_L

$$C_L = \frac{\rho_w g D_w}{\Delta \overline{T}} \frac{dT_m}{dp}(p_b) \tag{23}$$

Strategy

- spherical harmonics decomposition in lateral variables and finite differences in radius
- separation of time scales
- $Ek \in \{9\times10^{-4}, 6\times10^{-4}, 3\times10^{-4}\}$, $Pr = 10$
- $Ra = 3.3\times Pr\times Ek^{-12/7}$ $(R_G^* = 3.3)$
- $C_L \in \{0.3\times Nu, 0.8\times Nu\}$ and control run with homogeneous melting temperature along the boundary
- $r_s = 2575km$, $r_b = 2500km$, $r_c = 2000km$
- only a diffusion creep in ice viscosity

Results I

Figure: Ocean dynamics comparison. In the first row, the temperature deviation, zonal flows and radial velocities. In the second row the heat flux at the top of the ocean. From left to right: no boundary temperature variation, $C_L = 0.3Nu$, $C_L = 0.8Nu$

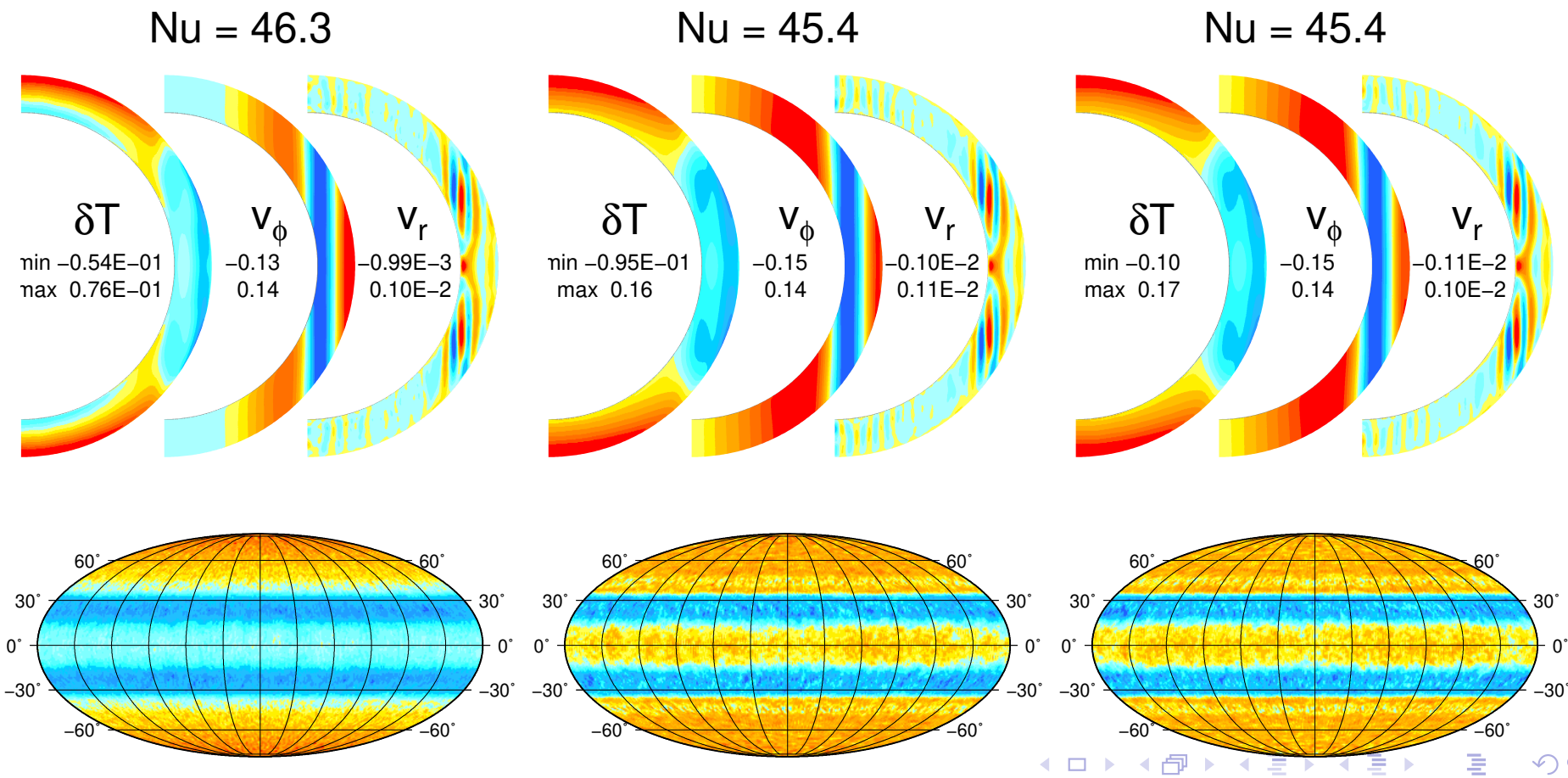

Results II

Figure: Ocean dynamics comparison. In the first row, the temperature deviation, zonal flows and radial velocities. In the second row the heat flux at the top of the ocean. $C_L = 0.3Nu$ in all cases.

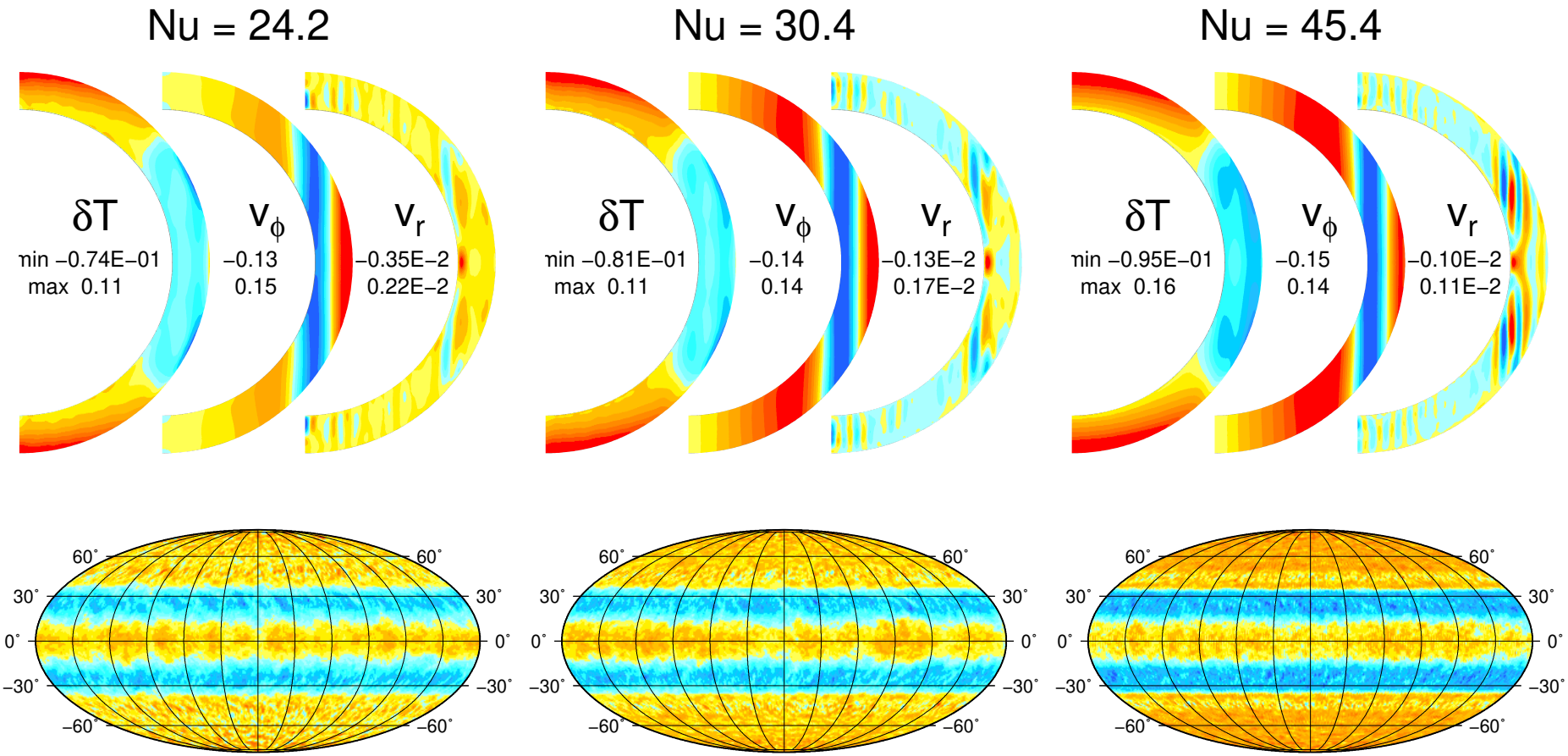

Results III

Figure: Topography (the first row) and shape (the second row) comparison. $Nu = 45.4$ in all cases. From left to right: no boundary temperature variation, $C_L = 0.3Nu$, $C_L = 0.8Nu$.

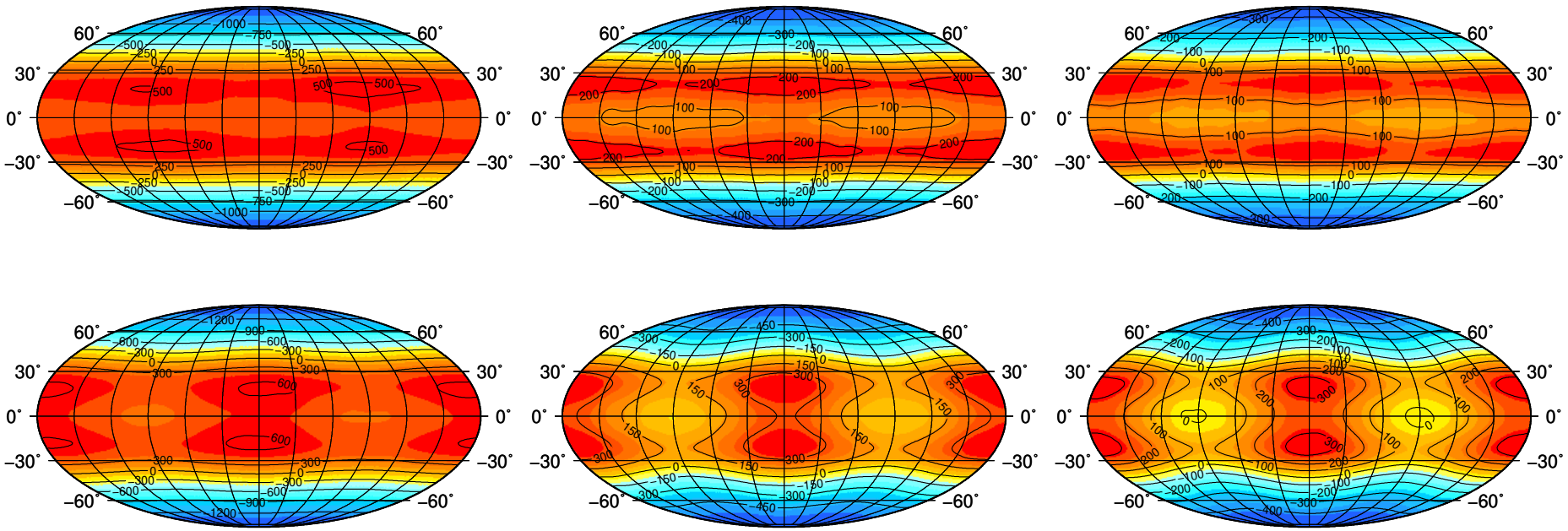

Results IV

Figure: Influence of the changes in melting temperature on zonal part of topography. Estimate on the Clayperon slope parameter for Titan reads $C_L = 0.0 - 0.3Nu$.

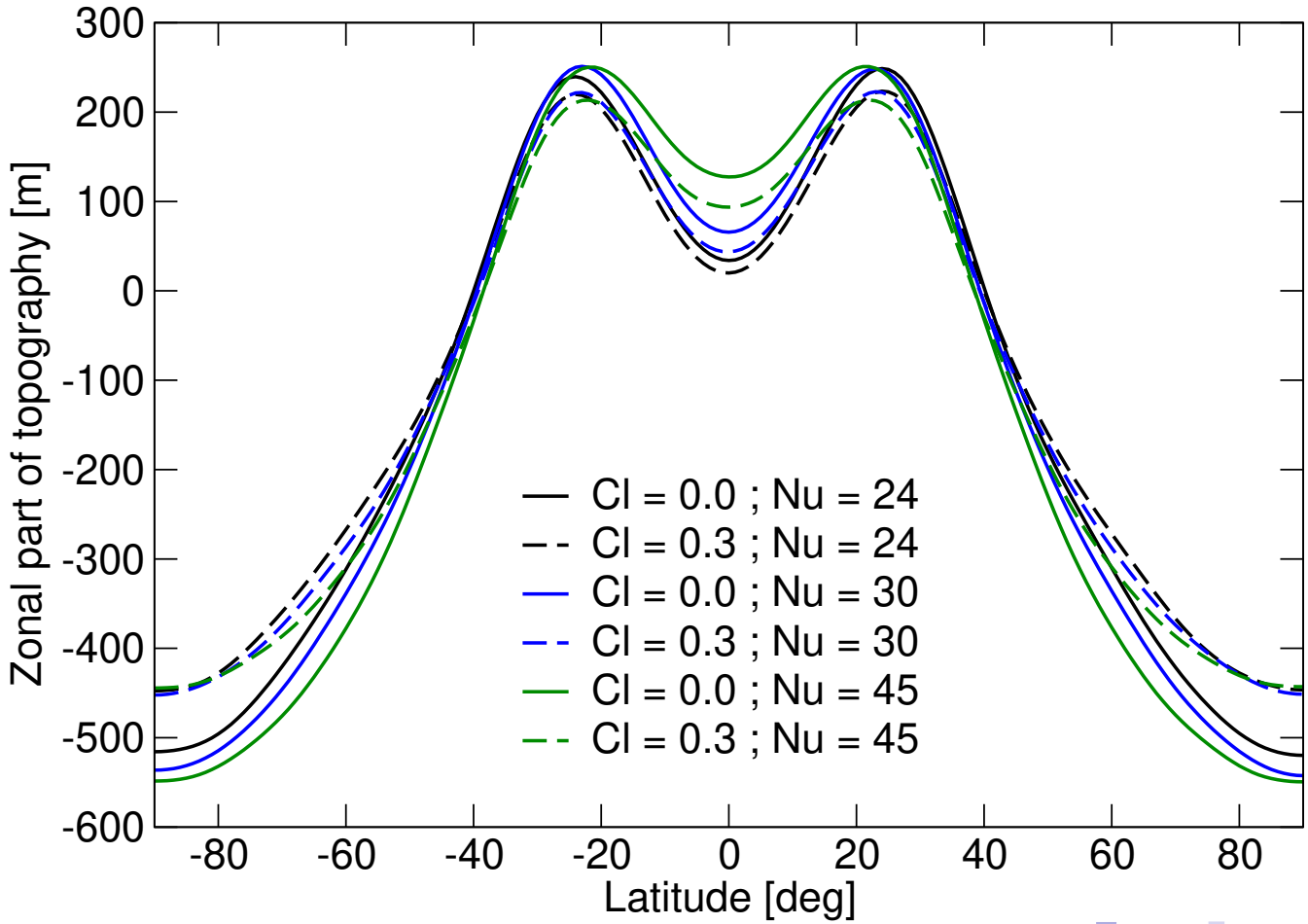

References I

H. Amit, G. Choblet, G. Tobie, F. Terra-Nova, O. Čadek, and M. Bouffard. Cooling patterns in rotating thin spherical shells — application to titan's subsurface ocean. *Icarus*, 338:113509, 2020. doi: 10.1016/j.icarus.2019.113509.

P. Corlies, A. G. Hayes, S. P. D. Birch, R. Lorenz, B. W. Stiles, R. Kirk, V. Poggiali, H. Zebker, and L. Iess. Titan's topography and shape at the end of the cassini mission. *Geophysical Research Letters*, 44(23): 11,754–11,761, 2017. doi: https://doi.org/10.1002/2017GL075518.

M. W. Dingemans. *Water Wave Propagation Over Uneven Bottoms, Part 1 - Linear wave propagation*. World Scientific Publishing Company, 1997. doi: 10.1142/1241.

D. Durante, D.J. Hemingway, P. Racioppa, L. Iess, and D.J. Stevenson. Titan's gravity field and interior structure after cassini. *Icarus*, 326: 123–132, 2019. doi: https://doi.org/10.1016/j.icarus.2019.03.003.

References II

T. Gastine, J. Wicht, and J. Aubert. Scaling regimes in spherical shell rotating convection. *Journal of Fluid Mechanics*, 808:690–732, 2016. doi: 10.1017/jfm.2016.659.

M. Kihoulou, O. Čadek, J. Kvorka, K. Kalousová, G. Choblet, and G. Tobie. Topographic response to ocean heat flux anomaly on the icy moons of Jupiter and Saturn. *Icarus*, 391:115337, 2023. doi: 10.1016/j.icarus.2022.115337.

J. Kvorka, O. Čadek, G. Tobie, and G. Choblet. Does Titan's long-wavelength topography contain information about subsurface ocean dynamics? *Icarus*, 310:149–164, 2018. doi: 10.1016/j.icarus.2017.12.010.

J. Kvorka and O. Čadek. A numerical model of convective heat transfer in titan's subsurface ocean. *Icarus*, 376:114853, 2022. doi: 10.1016/j.icarus.2021.114853.

References III

S. Labrosse, A. Morison, R. Deguen, and T. Alboussière. Rayleigh–bénard convection in a creeping solid with melting and freezing at either or both its horizontal boundaries. *Journal of Fluid Mechanics*, 846:5–36, 2018. doi: 10.1017/jfm.2018.258.

S. Schmitz and A. Tilgner. Heat transport in rotating convection without ekman layers. *Phys. Rev. E*, 80:015305, 2009. doi: 10.1103/PhysRevE.80.015305.

S. Schmitz and A. Tilgner. Transitions in turbulent rotating rayleigh-bénard convection. *Geophysical & Astrophysical Fluid Dynamics*, 104(5-6):481–489, 2010. doi: 10.1080/03091929.2010.504720.

J. C. Slattery, L. Sagis, and E.-S. Oh. *Interfaciel Transport Phenomena*. Springer New York, NY, 2007. ISBN 978-0-387-38442-9. doi: 10.1007/978-0-387-38442-9.

References IV

K. M. Soderlund. Ocean dynamics of outer solar system satellites. *Geophysical Research Letters*, 46:8700–8710, 2019. doi: 10.1029/2018GL081880.

O. Čadek, M. Běhounková, G. Tobie, and G. Choblet. Viscoelastic relaxation of enceladus's ice shell. *Icarus*, 291:31–35, 2017. doi: 10.1016/j.icarus.2017.03.011.

O. Čadek, O. Souček, M. Běhounková, G. Choblet, G. Tobie, and J. Hron. Long-term stability of enceladus' uneven ice shell. *Icarus*, 319:476–484, 2019. doi: 10.1016/j.icarus.2018.10.003.

O. Čadek, K. Kalousová, J. Kvorka, and C. Sotin. The density structure of titan's outer ice shell. *Icarus*, 364:114466, 2021. doi: 10.1016/j.icarus.2021.114466.